Supplementary Information

Intermediate Layer Modulation between NiCoP and Ni Foam Substrate in Microwire Array Electrode for Enhanced Hydrogen Evolution Reaction

Dan Guo,[#a] Huayu Chen,[#b,c] Hanmin Tian,*[a] Shuxin Ouyang,*[d] Jianbo Wang [e,g] and Jun Lv*[f,g]

[a] School of Electronics and Information Engineering, Hebei University of Technology, Tianjin 300400, P. R. China

[b] College of Materials and Chemistry, China Jiliang University, Hangzhou 310018, P. R. China.

[c] TJU-NIMS International Collaboration Laboratory, School of Materials Science and Engineering, Tianjin University, Tianjin 300072, P. R. China

[d] College of Chemistry, Central China Normal University, Wuhan 430079, P. R. China

[e] School of Electronic Science & Engineering, Southeast University, Nanjing 210096, P. R. China

[f] Electronic Information Engineering College, Sanjiang University, Nanjing 210012, P. R. China

[g] LONGi Solar Technology Co., Ltd., Xi'an 710018, P. R. China

[#] These authors contributed equally to this work.

*Author to whom correspondence should be addressed.
Email: tianhanmin@hebut.edu.cn; oysx@mail.ccnu.edu.cn; solar_lv@163.com

Experimental Section

Preparation of CoCH/NF and CoMoCH/NF Microwire Array Electrodes: The $Co(NO_3)_2 \cdot 6H_2O$ (0.582 g), NH_4F (0.186 g) and urea (0.60 g) were dissolved in 40 ml distilled water and stirred for 30 min to form a clear solution. In regard to the additive of NH_4F, the F^- ion can modulate the growth of crystal face, and NH_4^+ acts as complexing agent to modulate the polarity of solution and further affects mass transfer. A piece of Ni foam (2 cm × 3 cm) as the substrate was pretreated by alternatively stirred in 1 M H_2SO_4 aqueous solution and distilled water to remove the surface oxide. Subsequently the above mixed solution as well as the Ni foam substrate was transferred to a 50 ml Teflon-lined stainless steel autoclave and held at 120 °C for 6 h to deposit microwire array on the surface of Ni foam. After cooled down to room temperature, a piece of Ni foam coated with purple powder (denoted as CoCH/NF) was obtained. This CoCH/NF sample was washed by distilled water for several times and dried in vacuum.

For the preparation of CoMoCH/NF, the as-prepared CoCH/NF was immersed into a $Na_2MoO_4 \cdot 2H_2O$ aqueous solution (0.2 g dissolved in 35 ml distilled water) and then transferred to the 50 ml Teflon-lined stainless steel autoclave. After maintained at 120 °C for 6 h, the CoMoCH/NF with darker color was obtained.

Preparation of CoCH@NiCoP/NF and CoMoCH@NiCoP/NF Microwire Array Electrodes: The electrodepositions of NiCoP on the surfaces of CoCH/NF and CoMoCH/NF microwire array were operated by the electrochemical station (CHI 660E) in a three-electrode configuration. The electrolyte comprised of NH_4Cl (0.25 M), $NaH_2PO_4 \cdot H_2O$ (0.20 M), $NiCl_2 \cdot 6H_2O$ (0.20 M) and $CoCl_2 \cdot 6H_2O$ (0.20 M). The CoCH/NF (or CoMoCH/NF) was used as the work electrode, a Pt wire electrode was used as the counter electrode, and an Ag/AgCl (3 M KCl) electrode was used as the reference electrode. The CoCH/NF (or CoMoCH/NF) electrode was applied constant current of 30 mA for 40 min to finally form the CoCH@NiCoP/NF (or CoMoCH@NiCoP/NF) electrode. The mass loading of catalyst was about 3 mg cm^{-2}.

Characterizations: X-ray diffraction (XRD) patterns were measured by X-ray diffractometer (D8 Advanced, Bruker, Germany). The morphologies of the samples were observed by the transmission electron microscope (Jem-2100F, Jeol, Japan) and scanning electron microscope (S4800, Hitachi, Japan). The Brunauer-Emmett-Teller area was measured by nitrogen physisorption (Autosorb-iQ2, Quantachrome, America). Chemical valence analysis was performed by X-ray photoelectron spectroscopy (Escalab 250Xi, Thermo Scientific, America).

Electrochemical Measurements: Electrochemical activity was evaluated in a three-

electrode system in 1 M KOH aqueous solution by a CHI660e electrochemical workstation. The Ni foam loaded with as-prepared catalyst was used as the working electrode, a Pt wire electrode was used as the counter electrode, and an Ag/AgCl (3 M KCl) electrode was used as the reference electrode. All the potentials in this work were normalized to RHE according to the Nernst equation: E(RHE)=E(Ag/AgCl)+0.059×pH+0.198. The HER polarization activity was measured by linear sweep voltammetry (LSV) at the scan rate of 5 mV s^{-1}. The series resistance (R_s) values for iR correction were calculated using the results of electrochemical impedance spectroscopy (EIS) measurement. The EIS measurement was operated in the frequency range of 0.01 to 10^6 Hz at −0.057 V (vs RHE). I-t curve measurement was performed at a constant voltage of −0.102 V (vs RHE). The electrochemical active surface area (ECSA) was revealed by the electrochemical double-layer capacitance (C_{dl}) obtained from the cyclic voltammetry (CV) curves which were measured at different scan rates (20, 40, 80 ,120, 160 and 200 mV s^{-1}) at the non-Faradaic region (0.30 to 0.40 V vs RHE).

Photovoltaic-Water Splitting Application: The photovoltaic-electrocatalytic water splitting reaction was conducted in a water splitting reactor which was connected to a closed gas-circulation system (OLPCRS-3, Shanghai Boyi Scientific Instrument Co., China). The water splitting reaction was performed in 1 M KOH solution with the distance of 1 cm between the anode (IrO_2/NF) and cathode (CoMoCH@NiCoP/NF). The energy input was accomplished by a solar simulator (XES-50S1-RY, San-Ei Electric Co., Japan). The illumination area of the silicon film solar cell was optimized and the final energy input power was about 412 mW. The yields of H_2 and O_2 were detected by online gas chromatography (GC-2014C, Shimadzu Corp., Japan). The amount of H_2 was used to calculate the solar-to-hydrogen conversion efficiency (η_{STH}) for every hour through the following equal:

$$\eta_{STH} = \frac{\text{standard molar enthalpy of combustion (kJ mol}^{-1}) \times \text{H}_2 \text{ moles (mol)}}{\text{illumination power (W)} \times \text{time (s)}}$$

where the illumination power was measured by an optical power meter (PM 100D, Thorlabs, America), the range of measurement is 190 ~ 20000 nm, the energy of H_2 equals to the standard molar enthalpy of combustion (−285 kJ mol^{-1}).

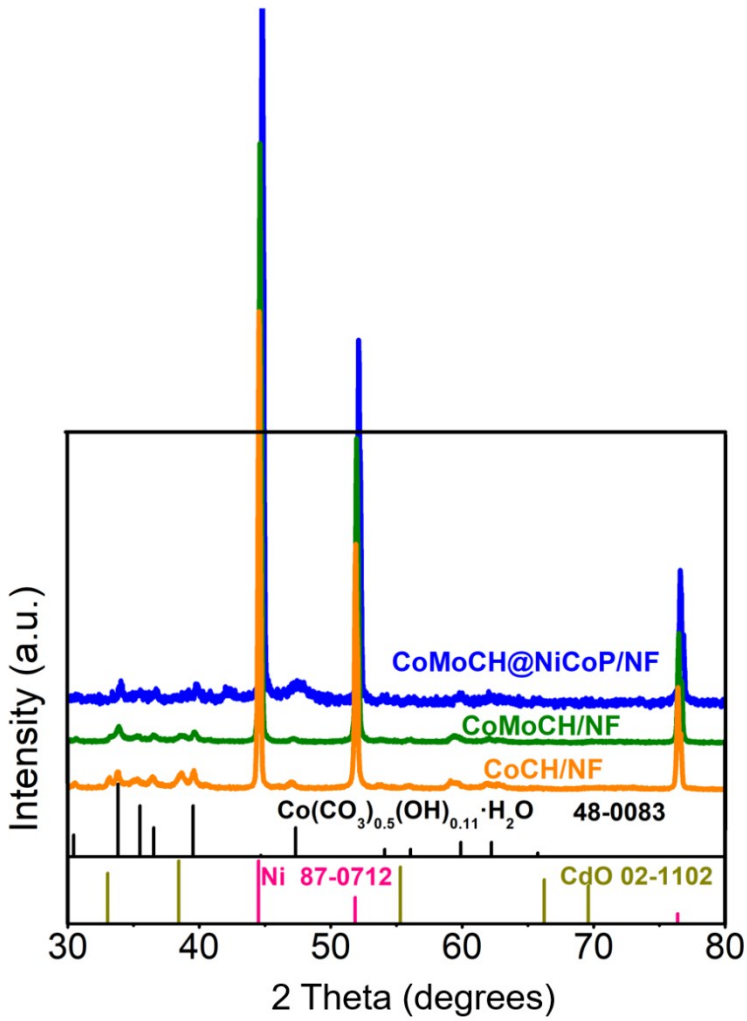

Fig. S1. Full XRD patterns of the samples.

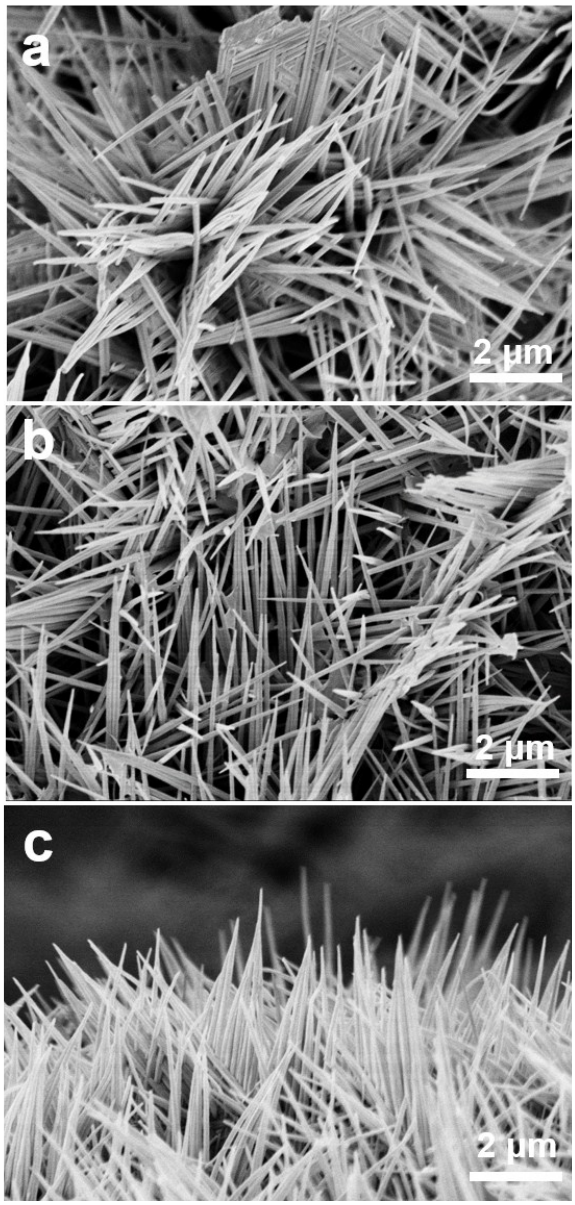

Fig. S2. SEM images of (a) CoCH/NF, (b) CoMoCH/NF and (c) CoCH@NiCoP/NF.

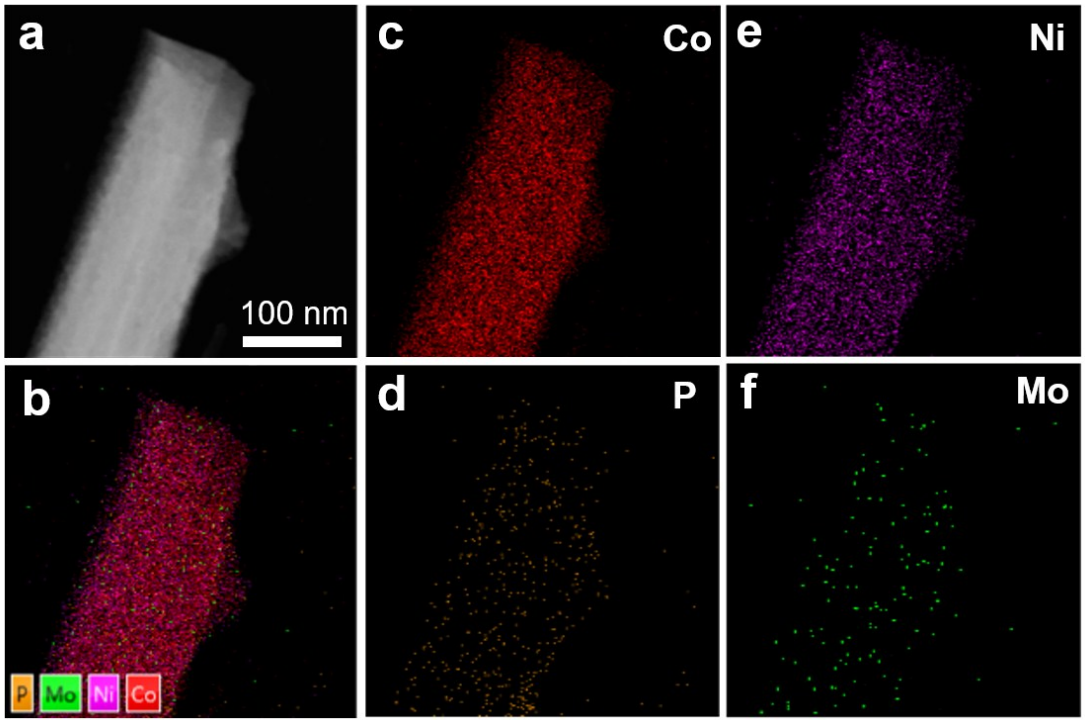

Fig. S3. (a) HAADF-STEM image, (b) combined element mapping image and (c-f) element mapping images of Co, P, Ni and Mo for the CoMoCH@NiCoP microwire.

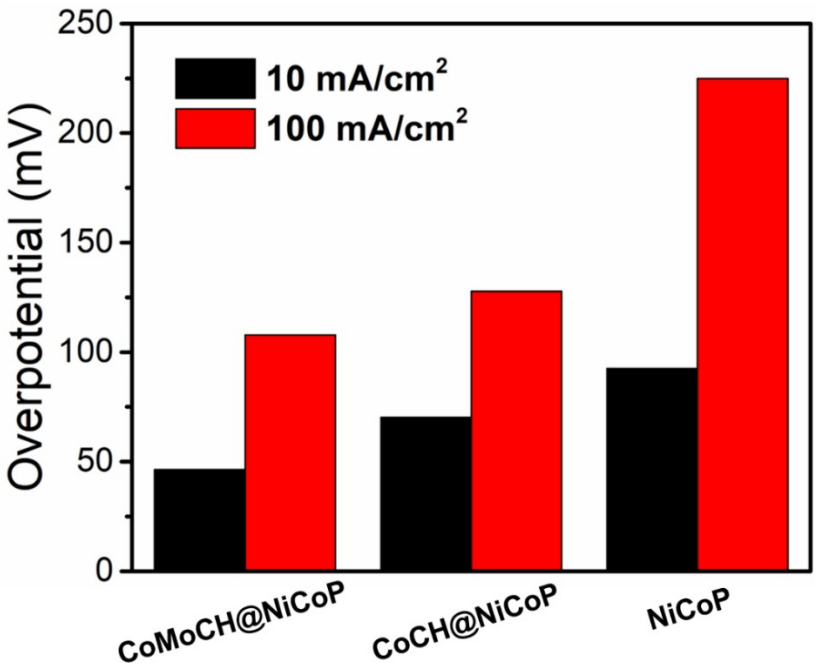

Fig. S4. Overpotentials obtained from HER polarization curves at the current density of 10 and 100 mA cm^{-2}.

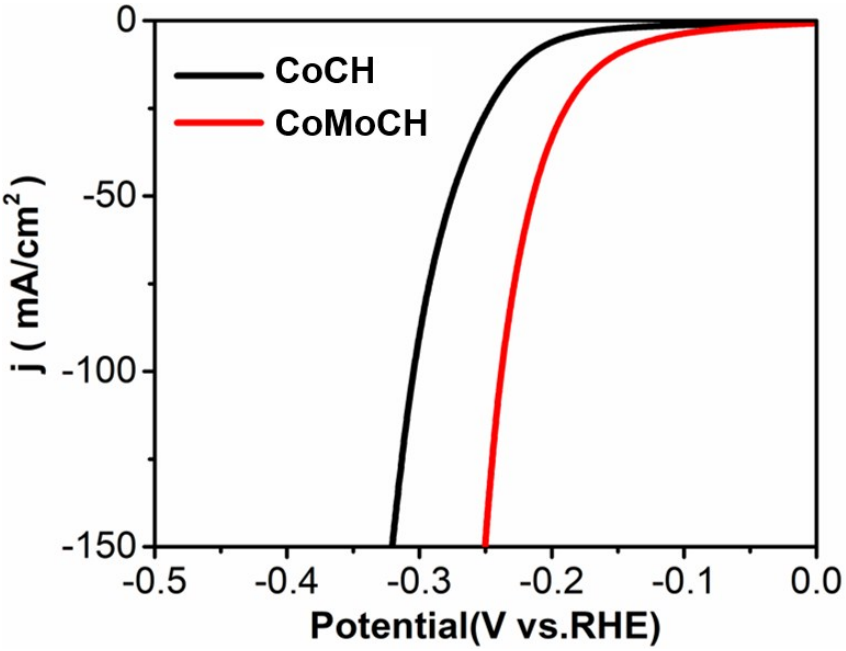

Fig. S5. LSV polarization curves of CoMoCH/NF and CoCH/NF electrodes.

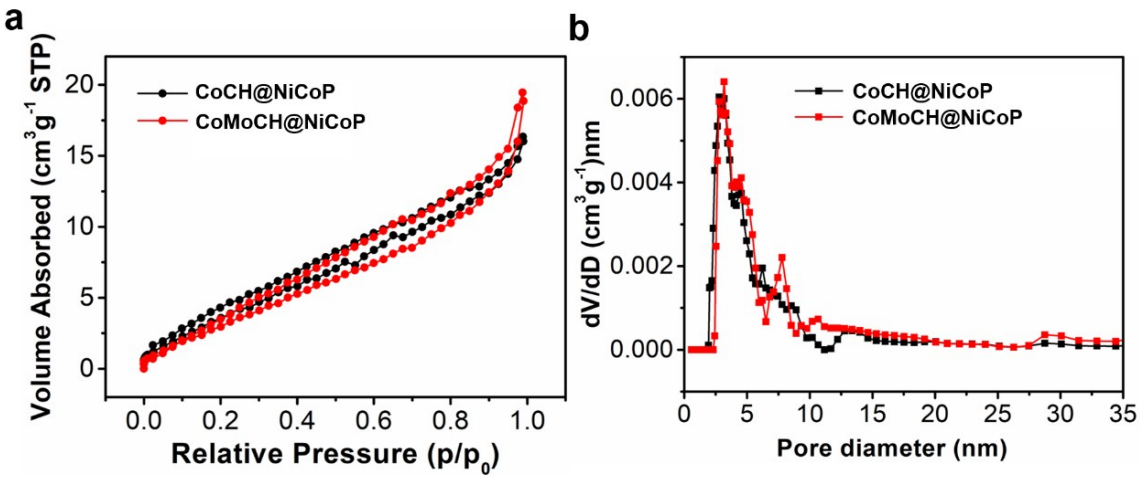

Fig. S6. (a) N_2 adsorption-desorption isotherms and (b) pore size distributions of the CoMoCH@NiCoP and CoCH@NiCoP catalysts.

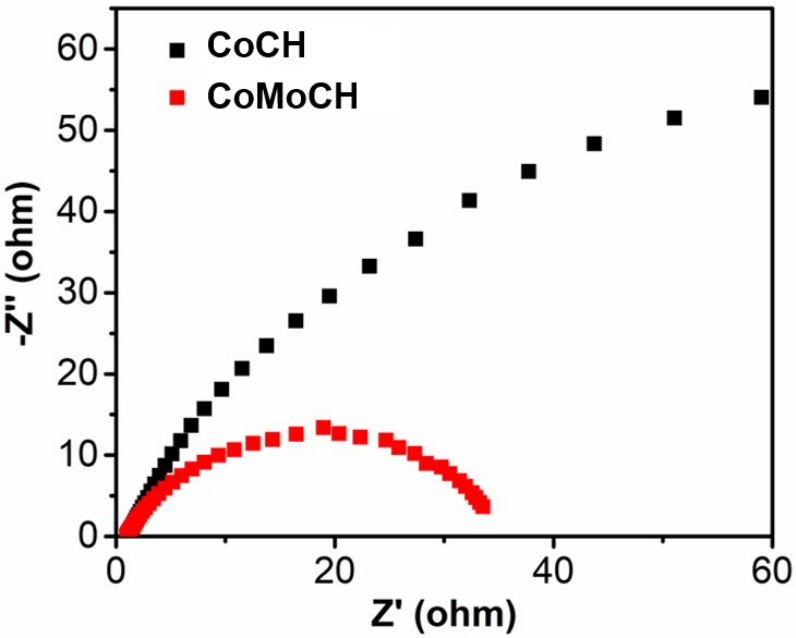

Fig. S7. Electrochemical impedance spectra measured at −0.06 V vs RHE for the CoMoCH/NF and CoCH/NF electrodes.

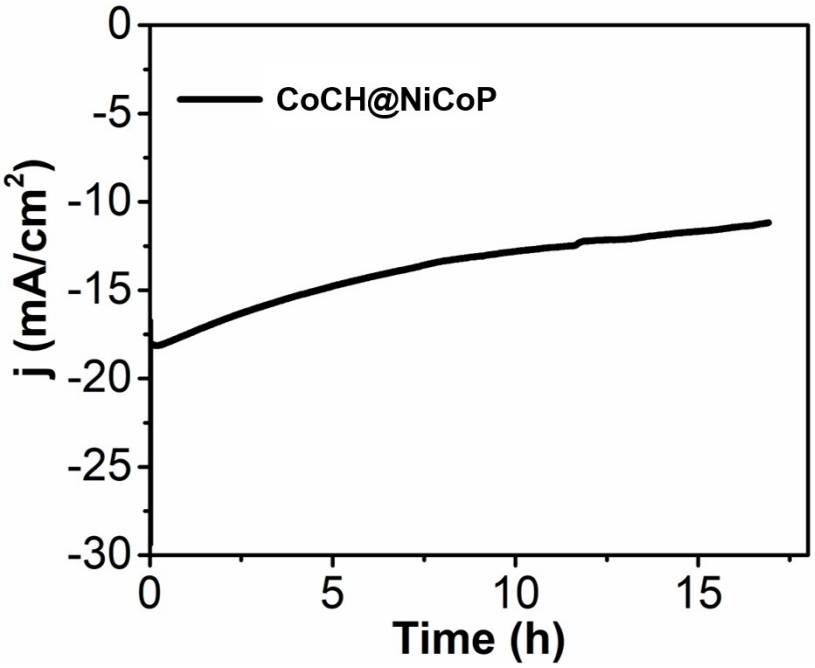

Fig. S8. Time-dependent current density curve for the CoCH@NiCoP/NF electrode.

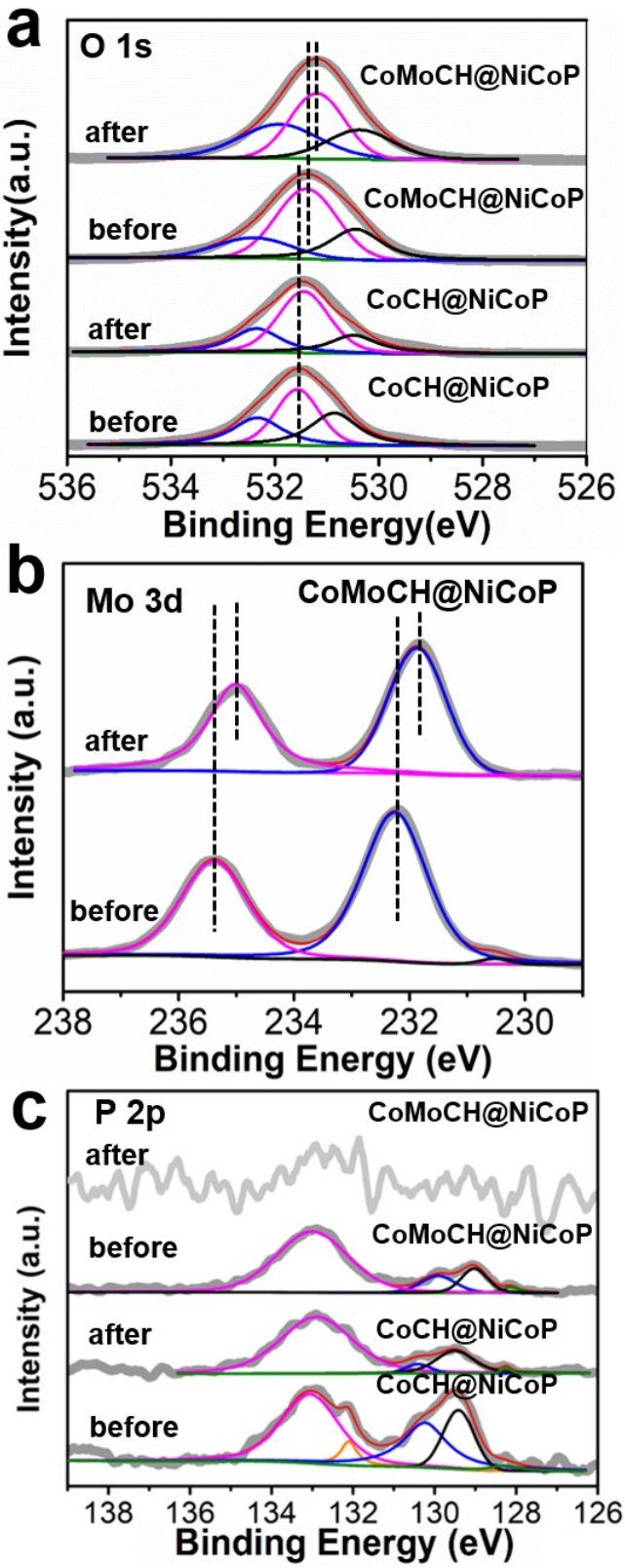

Fig. S9. XPS spectra of the (a) O 1s, (b) Mo 3d and (c) P 2p levels for the samples (before and after HER).

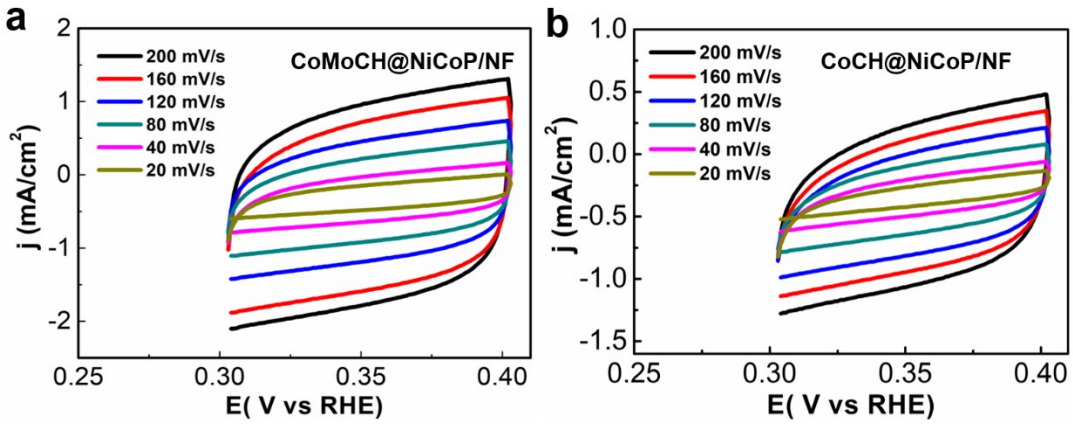

Fig. S10. CV curves of the (a) CoMoCH@NiCoP/NF and (b) CoCH@NiCoP/NF with various scan rates (20 ~ 200 mV s^{-1}) in the potential range of 0.30 ~ 0.40 V vs RHE.

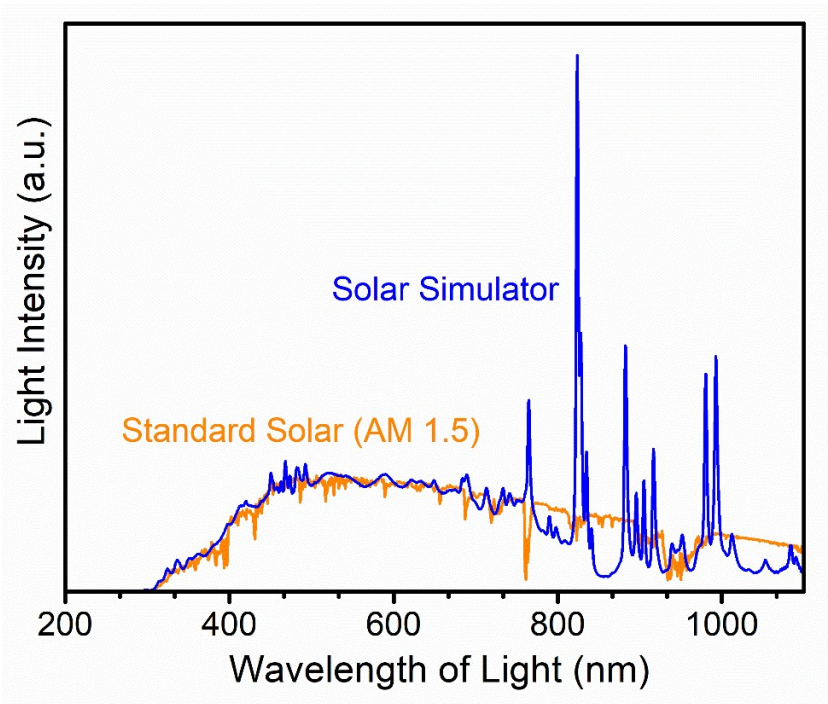

Fig. S11. The spectra of the input simulated sunlight and the standard AM 1.5 irradiation.

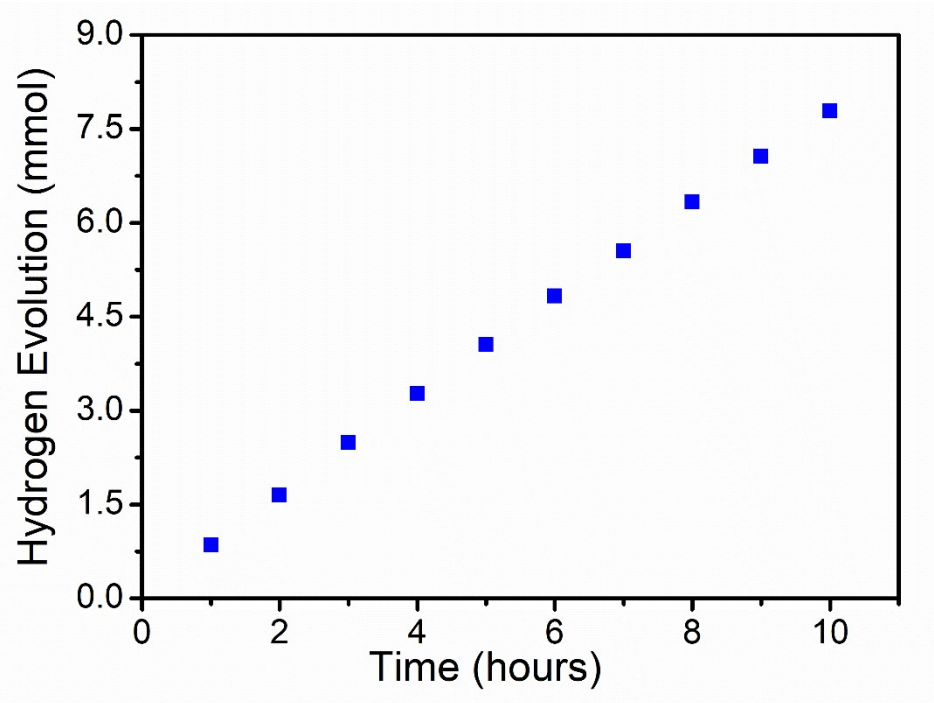

Fig. S12. The amount of H_2 evolution for the photovoltaic-water splitting device during the test lasted for 10 h.

Table S1. Element compositions of the CoMoCH@NiCoP/NF from XPS data.

Element	Peak BE	Height CPS	Atomic %
C 1s	284.79	15478.56	17.54
Co 2p	781.42	71341.47	13.76
O 1s	531.33	194691.82	56.02
Mo 3d	232.21	32352.67	2.53
Ni 2p	856.29	47358.87	7.98
P 2p	132.95	3095.85	2.17

Table S2. HER performance for the CoMoCH@NiCoP/NF electrode and the state-of-art electrocatalysts.

Catalyst	Morphology	Support	Electrolyte	η(mV)	j(mA cm^{-2})	Reference
NCP@MoCoCH	Nanowire array	Ni foam	1.0 M KOH	45 mV	10	This work
Pt/C	-	-	0.5 M H_2SO_4 1.0 M KOH	25 mV 43 mV	10	1
$CoMoO_4$	Nanowire array	Ti mesh	1.0 M KOH	81 mV	10	2
Co-Mo-B	amorphous film	Ti mesh	1.0 M KOH	110 mV	20	3
NiCoMo film	3D dendeitic structures	Ti sheet	0.5 M H_2SO_4 0.1 M KOH	35 mV 132 mV	10	4
Co-Mo/Ti	Nanoparticles	Ti foil	1.0 M KOH	75 mV	10	5
Mo-Fe (1/1)-Se	Nanosheet	Carbon paper	0.5 M H_2SO_4	86.9 mV	10	6
N, P-Mo_xC	Nanofibers	Ni foam	1.0 M KOH 0.5 M H_2SO_4	107 mV 135 mV	10	7
Mo_XC-Ni@NCV	Nanoparticles	Glassy carbon	0.5 M H_2SO_4	68 mV	10	8
MoO_x/Ni_3S_2/NF	Hollow microspheres	Ni foam	1.0 M KOH	106 mV	10	9

MoS_2/NiS/MoO_3	Nanowire	Ti foil	1.0 M KOH	91 mV	10	10
CoP	Nanoneedle arrays	Carbon cloth	1.0 M KOH	95 mV	10	11
Co/Co_3O_4	Nanosheets	Ni foam	1.0 M KOH	90 mV	10	12
MoP sheets	Nanosheet	Glassy carbon	0.5 M H_2SO_4	172 mV	10	13
Ni-C-N NSs	Nanosheets	Glassy carbon	0.5 M H_2SO_4 1.0 M KOH 1.0 M PBS	60.9 mV 30.8 mV 92.1 mV	10	14
FeP_2	Nanowire array	Fe foil	1.0 M KOH 0.5 M H_2SO_4	189 mV 61 mV	10	15
Co-P	Nanophere arrays	FTO	1.0 M KOH	125 mV	10	16
Co-P	Foam structure	Copper sheet	0.5 M H_2SO_4 1.0 M KOH	50 mV 131 mV	10	17
Co_{59}-P_{20}-B_{21}	amorphous	Carbon paper	0.5 M H_2SO_4	172 mV	10	18
Fe_{10}-Co_{40}-Ni_{40}-P	Nanosheet arrays	Ni foam	1.0 M KOH	68 mV	10	19
$Fe_{0.5}Co_{0.5}P$	Nanowire array	Carbon cloth	0.5 M H_2SO_4	37 mV	10	20

$NiSe_2$ NTAS	Nanotube arrays	Ni foam	1.0 M KOH 0.5 M H_2SO_4	60 mV 98 mV	10	21
CC@N-CoP	Nanowire array	Carbon cloth	0.5 M H_2SO_4	42 mV	10	22
PANI/CoP HNWs-CFs	nanowires	Carbon fibers	0.5 M H_2SO_4	57 mV	10	23
$(Ni.Co)_{0.85}Se$	Nanosheet arrays	Ni foam	1.0 M KOH	169 mV	10	24
Ni_x P/NF-20	nanospheres	Ni foam	1.0 M KOH	63 mV	10	25
Ni3N@CQDs	Nanosheet	Glassy carbon	1.0 M KOH	69 mV	10	26
FeP/C with shell	nanoparticles	Glassy carbon	0.5 M H_2SO_4	71 mV	10	27
$Zn_{0.08}Co_{0.92}P$/TM	Nanowall array	Ti mesh	1.0 M KOH 0.5 M H_2SO_4	67 mV 39 mV	10	28
Mn-Ni_2P/NF	Nanosheet array	Ni foam	1.0 M KOH	103 mV	20	29
Al-CoP/CC	nanoarray	Carbon cloth	0.5 M H_2SO_4	23 mV	10	30
Al-Ni_2P	Nanosheet array	Ti mesh	1.0 M KOH	129 mV	10	31

Reference

1. B. Liu, L. Huo, Z. Gao, G. Zhi, G. Zhang and J. Zhang, *Small*, 2017, **13**, 1700092.

2. J. Zhao, X. Ren, H. Ma, X. Sun, Y. Zhang, T. Yan, Q. Wei and D. Wu, *ACS Sustain. Chem. Eng.*, 2017, **5**, 10093-10098.
3. Z. Sun, S. Hao, X. Ji, X. Zheng, J. Xie, X. Li and B. Tang, *Dalton T.*, 2018, **47**, 7640-7643.
4. D. Gao, J. Guo, X. Cui, L. Yang, Y. Yang, H. He, P. Xiao and Y. Zhang, *ACS Appl. Mater. Interfaces*, 2017, **9**, 22420-22431.
5. J. M. McEnaney, T. L. Soucy, J. M. Hodges, J. F. Callejas, J. S. Mondschein and R. E. Schaak, *J. Mater. Chem. A*, 2016, **4**, 3077-3081.
6. Y. Chen, J. Zhang, P. Guo, H. Liu, Z. Wang, M. Liu, T. Zhang, S. Wang, Y. Zhou, X. Lu and J. Zhang, *ACS Appl. Mater. Interfaces*, 2018, **10**, 27787-27794.
7. L. Ji, J. Wang, X. Teng, H. Dong, X. He and Z. Chen, *ACS Appl. Mater. Interfaces*, 2018, **10**, 14632-14640.
8. S. Wang, J. Wang, M. Zhu, X. Bao, B. Xiao, D. Su, H. Li and Y. Wang, *J. Am. Chem. Soc.*, 2015, **137**, 15753-15759.
9. Y. Wu, G.-D. Li, Y. Liu, L. Yang, X. Lian, T. Asefa and X. Zou, *Adv. Funct. Mater.*, 2016, **26**, 4839-4847.
10. C. Wang, B. Tian, M. Wu and J. Wang, *ACS Appl. Mater. Interfaces*, 2017, **9**, 7084-7090.
11. P. Wang, F. Song, R. Amal, Y. H. Ng and X. Hu, *ChemSusChem*, 2016, **9**, 472-477.
12. X. Yan, L. Tian, M. He and X. Chen, *Nano Lett.*, 2015, **15**, 6015-6021.
13. J. Jia, W. Zhou, G. Li, L. Yang, Z. Wei, L. Cao, Y. Wu, K. Zhou and S. Chen, *ACS Appl. Mater. Interfaces*, 2017, **9**, 8041-8046.
14. J. Yin, Q. Fan, Y. Li, F. Cheng, P. Zhou, P. Xi and S. Sun, *J. Am. Chem. Soc.*, 2016, **138**, 14546-14549.
15. C. Y. Son, I. H. Kwak, Y. R. Lim and J. Park, *Chem. Commun.*, 2016, **52**, 2819-2822.
16. G.-Q. Han, X. Li, Y.-R. Liu, B. Dong, W.-H. Hu, X. Shang, X. Zhao, Y.-M. Chai, Y.-Q. Liu and C.-G. Liu, *RSC Adv.*, 2016, **6**, 52761-52771.
17. S. Oh, H. Kim, Y. Kwon, M. Kim, E. Cho and H. Kwon, *J. Mater. Chem. A*, 2016, **4**, 18272-18277.
18. J. Kim, H. Kim, S.-K. Kim and S. H. Ahn, *J. Mater. Chem. A*, 2018, **6**, 6282-6288.
19. Z. Zhang, J. Hao, W. Yang and J. Tang, *RSC Adv.*, 2016, **6**, 9647-9655.
20. C. Tang, L. Gan, R. Zhang, W. Lu, X. Jiang, A. M. Asiri, X. Sun, J. Wang and L. Chen, *Nano Lett.*, 2016, **16**, 6617-6621.
21. X. Teng, J. Wang, L. Ji, Y. Lv and Z. Chen, *Nanoscale*, 2018, **10**, 9276-9285.
22. Q. Zhou, Z. Shen, C. Zhu, J. Li, Z. Ding, P. Wang, F. Pan, Z. Zhang, H. Ma, S. Wang and H. Zhang, *Adv. Mater.*, 2018, **30**, e1800140.
23. J. X. Feng, S. Y. Tong, Y. X. Tong and G. R. Li, *J. Am. Chem. Soc.*, 2018, **140**, 5118-5126.
24. K. Xiao, L. Zhou, M. Shao and M. Wei, *J. Mater. Chem. A*, 2018, **6**, 7585-7591.
25. X. Cao, D. Jia, D. Li, L. Cui and J. Liu, *Chem. Eng. J.*, 2018, **348**, 310-318.
26. M. Zhou, Q. Weng, Z. I. Popov, Y. Yang, L. Y. Antipina, P. B. Sorokin, X. Wang, Y. Bando and D. Golberg, *ACS Nano*, 2018, **12**, 4148-4155.
27. D. Y. Chung, S. W. Jun, G. Yoon, H. Kim, J. M. Yoo, K. S. Lee, T. Kim, H. Shin, A. K. Sinha, S. G. Kwon, K. Kang, T. Hyeon and Y. E. Sung, *J. Am. Chem. Soc.*, 2017, **139**, 6669-6674.
28. T. Liu, D. Liu, F. Qu, D. Wang, L. Zhang, R. Ge, S. Hao, Y. Ma, G. Du, A. M. Asiri, L. Chen and X. Sun, *Adv. Energy Mater.*, 2017, **7**.
29. Y. Zhang, Y. Liu, M. Ma, X. Ren, Z. Liu, G. Du, A. M. Asiri and X. Sun, *Chem. Commun.*,

2017, **53**, 11048-11051.
30. Z. Xiong, Z. Lei, C.-C. Kuang, X. Chen, B. Gong, Y. Zhao, J. Zhang, C. Zheng and J. C. S. Wu, *Applied Catalysis B-Environmental*, 2017, **202**, 695-703.
31. H. Du, L. Xia, S. Zhu, F. Qu and F. Qu, *Chem Commun (Camb)*, 2018, **54**, 2894-2897.